Polymer Chemistry

Synthesis of poly(caprolactone)-*block*-poly[oligo(ethylene glycol) methyl methacrylate] amphiphilic grafted nanoparticles (AGNs) as improved oil dispersants

Journal:	*Polymer Chemistry*
Manuscript ID	PY-ART-03-2021-000418.R1
Article Type:	Paper
Date Submitted by the Author:	08-Jun-2021
Complete List of Authors:	Keller, Christopher; Tulane University, Chemistry Department Walley, Susan; University of Florida, Department of Chemistry Jarand, Curtis; Tulane University of Louisiana, Department of Physics He, JiBao; Tulane University, Coordinated Instrument Facility Ejaz, Muhammad; Tulane University, Department of Chemistry Savin, Daniel; University of Florida, Chemistry Grayson, Scott; Tulane University, Chemistry

ARTICLE

Synthesis of poly(caprolactone)-*block*-poly[oligo (ethylene glycol) methyl methacrylate] amphiphilic grafted nanoparticles (AGNs) as improved oil dispersants

Received 00th January 20xx,
Accepted 00th January 20xx

DOI: 10.1039/x0xx00000x

Christopher B. Keller[*a], Susan E. Walley[d], Curtis W. Jarand[b], Jibao He[c], Muhammad Ejaz[a], Daniel A. Savin[d], and Scott M. Grayson[a]

Linear-bottlebrush, amphiphilic copolymers were grafted from the surface of silica (SiO_2) nanoparticles to form "nanoparticle micelles" that, regardless of the concentration, possess the capability to encapsulate and stabilize non-polar structures in aqueous media. These nanoparticles afford high water dispersibility and enhanced oil encapsulation from their inherent architectural design. Utilizing well-established techniques, such as surface-initiated ring-opening polymerization (SI-ROP) and surface-initiated atom transfer radical polymerization (SI-ATRP), to effectively fine-tune the ratio of hydrophobic (poly(caprolactone), PCL) to hydrophilic (poly[oligo(ethylene glycol) methyl methacrylate mono-methyl ether], POEGMA) copolymer composition, enhances oil encapsulation while maintaining aqueous solubility. Preliminary oil encapsulation was quantified with differential scanning calorimetry (DSC) using two different types of crude oil. These nanoparticles offer an alternative dispersant system to replace commercially used Corexit™ 9500 by effectively breaking up disastrous oil slicks and minimizing the long-term effects of dispersant additives in the environment.

Introduction

The need for a robust replacement for commercially used dispersants has been an interest of oil spill preventative research since the Deepwater Horizon oil spill.[1–8] Traditionally, surfactant systems, such as Corexit™ 9500, are used as the dispersant for industrial oil spills.[8–10] These surfactant systems have shown self-assembly in aqueous solution under high agitation due to the amphiphilic nature of their chemical components.[8] However, Corexit™ 9500 encapsulates oil microdroplets briefly due to its dependence on critical micelle concentration (CMC).[8,11] Below the CMC of Corexit™ 9500 (22.5 mg L^{-1}),[11] self-assemblies generated from the surfactant components become too dilute and disassemble,[12] causing the oil to recoalesce at the air-water interface. From a practical standpoint, this means that an extremely large excess of material, many millions of liters, would be needed to clean an oil spill in an ocean setting due to the inherent volume of water being treated. In the case of the Deepwater Horizon Oil Spill approximately 8 million liters of Corexit™ 9500 was applied to the Gulf of Mexico,[11] and quickly became diluted below the cmc.

[a] *Department of Chemistry, Percival Stern Hall, Tulane University, New Orleans, Louisiana, 70118*
[b] *Department of Physics and Engineering Physics, Percival Stern Hall, Tulane University, New Orleans, Louisiana, 70118*
[c] *Coordinated Instrument Facility, Percival Stern Hall, Tulane University, New Orleans, Louisiana, 70118*
[d] *Department of Chemistry, Leigh Hall, University of Florida, Gainesville, Florida 32611*
[e] *Electronic Supplementary Information (ESI) available: [TEM images of SiO_2-GPS-PCL-POEGMA-Br steps; TGA plots with first weight % derivatives of SiO_2-GPS-PCL-POEGMA-Br steps; TGA plots with first weight % derivative of ungrafted PCL and POEGMA controls; ^1H and ^{13}C NMR of ε-caprolactone monomer; ^1H and ^{13}C NMR of ungrafted water-initiated poly(caprolactone); ^1H and ^{13}C NMR of ethyl 2-bromoisobutyrate (EBiB); ^1H and ^{13}C NMR of ungrafted EBiB-initiated POEGMA; TGA plots with first weight % derivatives of SiO_2-GPS-PCL-POEGMA-Br NPs; DSC plot of SiO_2-GPS-PCL-POEGMA-Br NPs before and after exposure to Anadarko crude oil.]. See DOI: 10.1039/x0xx00000x*

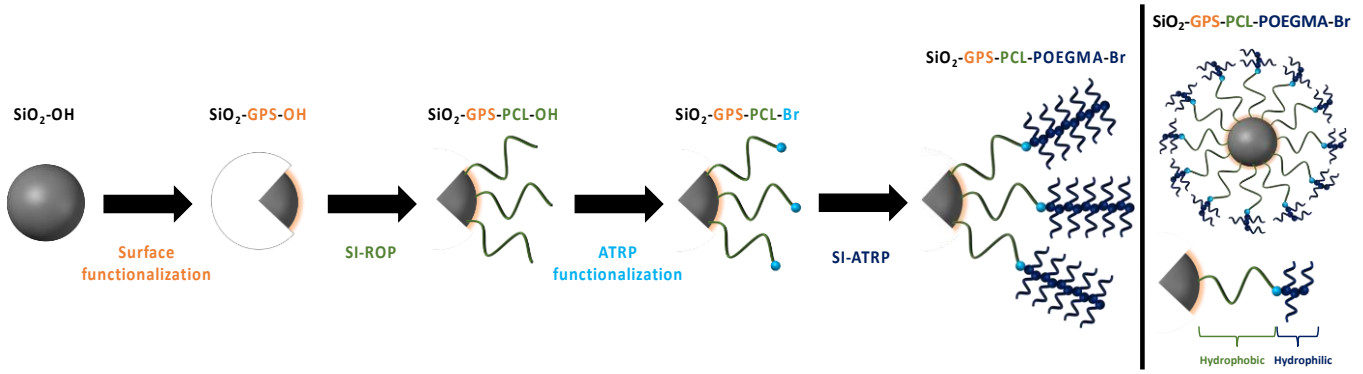

Figure 1: Representative synthetic scheme illustrating the grafted linear-bottlebrush polymers involving hydroxy functionalization of the silica nanoparticles (orange), SI-ROP addition of PCL (green), post-polymerization ATRP functionalization of PCL (light blue), and SI-ATRP addition of POEGMA (dark blue). A representation of the surface coverage of polymers on the nanoparticles with hydrophobic (green) PCL, and hydrophilic (dark blue) POEGMA

Within the literature, alternate dispersant systems to Corexit™ 9500 have been demonstrated where amphiphilic copolymers are covalently bound to a central junction point, and a "unimolecular-micelle"[5,6,21–24,13–20] inspired nanoparticle system can be synthetically generated. Traditionally, polymers are attached to the surface of nanoparticles using either a "graft-to"[14–18] or "graft-from"[25,26,35–37,27–34] approach. While both these approaches are equally valid, "graft-from" is typically preferred as it leads to higher grafting densities. Unlike "graft-to", the polymers generated from the "graft-from" approach cannot be fully characterized before addition to the nanoparticle surface, because the polymer chains are grown directly from the initiator immobilized on the surface. By covalently grafting amphiphilic copolymers from the surface of nanoparticles,[1,2,42,4–6,24,38–41] the non-polar, interior block allows for encapsulation and dispersion of the hydrophobic oil while the hydrophilic, outer corona block maintains aqueous dispersibility. Combining these two blocks onto a nanoparticle prevents disassembly and release of the oil, regardless of the volume of water. Pavia-Sanders et al. synthesized a series of grafted poly(acrylic acid)-*block*-poly(styrene) (PAA-*b*-PS) Fe_3O_4 magnetic nanoparticle dispersants as an effective mechanism for cleanup after the oil was sequestered.[4] Ejaz et al. synthesized a series of polymer-grafted nanoparticle systems as dispersants, with two systems in particular using variations of poly(caprolactone)-*block*-poly(ethylene glycol) (PCL-*b*-PEG)[5] and poly(caprolactone)-*block*-hyperbranched poly(glycidol) (PCL-*b*-HPG)[6] copolymers. Neither the particles generated by Pavia-Sanders et al. or Ejaz et al. had a noted cmc dependence, contrasting the primary limitation of Corexit™ 9500.

In the work of Ejaz et al., linear PEG[5] was modified through Jones oxidation to be used as the hydrophilic block. While this made the nanoparticles water dispersible, this design can be improved by utilizing fewer harsh synthetic steps and exploiting the architectural properties of having multiple PEG sidechains from a single backbone, or bottlebrush PEG represented in Figure 1. The combination of silica nanoparticles, PCL, and POEGMA will provide such an enhanced amphiphilic system.

Theoretically, the interior, linear PCL chain is collapsed under aqueous conditions and expands as it encapsulates oil. It stands to reason that as the length of the grafted PCL chain increases, this also increases the potential for higher oil loading. While PCL facilitates oil uptake, the exterior, bottlebrush POEGMA chain allows the nanoparticles to remain dispersed in water. Room temperature SI-ROP reactive conditions have been established by Lohmeijer et al. providing a means to graft high molecular weight PCL from the surface of functionalized silica nanoparticles.[43,44] Further, oligo(ethylene glycol) methyl methacrylate mono-methyl ether (OEGMA) monomers can be easily tailored to fit the need of precise block lengths due to extensive ATRP work of POEGMA in the literature.[13,15,41,45–51,18,24,25,27–30,39] Namely, the ratio of hydrophobic to hydrophilic monomers in these amphiphilic copolymers can be adjusted through monomer loading and mild reaction steps, using the established techniques of surface-initiated ring opening polymerization (SI-ROP) and surface-initiated atom transfer radical polymerization (SI-ATRP). Herein we report amphiphilic systems that are covalently grafted from the surface of silica nanoparticles with a long, linear, interior hydrophobic block and a short, bulky, exterior hydrophilic block. The amphiphilic grafted nanoparticles possess a "CMC" value, but it is an order of magnitude lower than the CMC of Corexit™. The proposed work below focuses on the "graft-from" approach and mild reaction conditions to sequentially graft PCL-b-POEGMA copolymers from the surface of silica nanoparticles, providing much higher oil encapsulation in water.

Experimental

Chemicals and Reagents

Snowtex-ZL silica suspension (Lot #240703) was provided

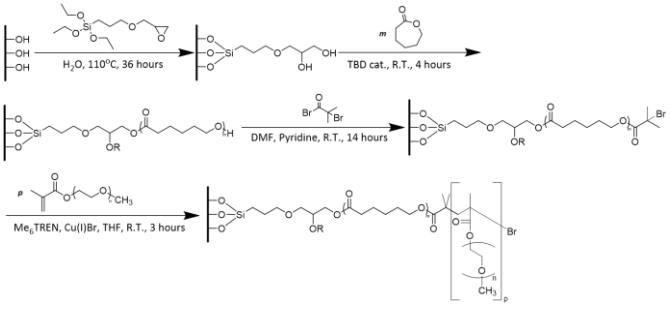

Scheme 1: Synthesis of SiO_2-GPS-PCL-POEGMA-Br amphiphilic grafted nanoparticles, where R represents an identical growing polymer chain

by Nissan Chemical Industries, LTD at 30% by weight of colloidal silica nanoparticles (SiO_2 NP, R_h = 50-75 nm) in water. The SiO_2 nanoparticles were collected via centrifugation at 14k revolutions per minute (RPM) for 30 min at 10˚C. The solid SiO_2 nanoparticles were subsequently dispersed in methanol before additional centrifugation at 14k RPM for 30 min at 10˚C before drying under high vacuum for 14 h at 25˚C. Sodium hydroxide pellets (97%, Fisher Scientific) were dissolved in deionized water to a concentration of 0.1 M. ε-Caprolactone (>99%, TCI America) was dried with CaH_2 for 14 h, followed by reduced pressure distillation at 120˚C. Oligo(ethylene glycol) methyl methacrylate mono-methyl ether (OEGMA, >99%, Sigma-Aldrich America, M_n 500) was passed over a column of activated basic aluminum oxide (Al_2O_3, 50-200 μm) to remove any inhibitor. A Welch 1400 vacuum pump was used in tandem with a Schlenk line apparatus to dry the nanoparticles at each step, for flame-drying glassware, freeze-pump-thaw cycles, and to purify any chemicals. A Beckman Coulter Avanti JXN-30 centrifuge was used for washing the nanoparticles in a variety of solvents at 14k RPM for 30 min at 10˚C. (3-Glycidoxypropyl)triethoxysilane (GPS, >95%, Gelest America), 1,5,7-triazabicyclo[4.4.0]dec-5-ene (TBD, 98%, Sigma-Aldrich America), tris[2-(dimethylamino)ethyl]amine (Me_6TREN, >98%, TCI America), ethyl α-bromoisobutyrate (EBiB, >98%, TCI America), and α-bromoisobutyryl bromide (BiBB, >98%, TCI America) were used as received.

Immobilization of GPS on the Surface of SiO_2-OH NPs (SiO_2-GPS-OH NPs), 1

Dispersed SiO_2 NPs (30% by weight in water) were centrifuged down at 14k RPM for 30 min. The solvent was decanted, deionized water was added, the nanoparticles were dispersed via sonication, and this step was repeated five additional times. The nanoparticles were diluted one additional time with deionized water to a concentration of 21.1 g SiO_2 NP in 71.0 g H_2O (30 wt. %) from the original concentration supplied by the manufacturer. The SiO_2 NP suspension was added to a 2-neck, 250 mL round bottom flask equipped with a poly(tetrafluoroethylene) (PTFE), magnetic stir bar and reflux condenser. 24.4 g (0.09 mol) GPS was added via syringe, then the suspension was diluted with deionized water to a concentration of 0.2 g mL^{-1} (20 wt. %) SiO_2 NP in water. The pH was brought to pH 10-12 through the dropwise addition of 0.1M aqueous sodium hydroxide solution. The suspension was refluxed at 110˚C for 36 h. The reaction was quenched by cooling to room temperature, then sonicating in pH neutral deionized water for 10 min. Work up consisted of centrifuge and decant cycles in pH 7 DIW and repeated until neutral pH is reached. The nanoparticles were then dispersed in methanol, centrifuged for an additional three to five cycles, and dried at room temperature overnight (14 h) under high vacuum. The reaction yielded 16.9 g of product, at a 98.58% yield calculated from TGA percent weight change from previous SiO_2-OH NPs. TGA: 1.37% (25 to 600˚C) increase by weight from bare SiO_2 NPs; FTIR: 3400-3000 cm^{-1} (ν O-H), 2930 cm^{-1} (ν_{as} C-H), 2866 cm^{-1} (ν_s C-H), 1250-950 cm^{-1} (ν Si-O(Si)), 850-775 cm^{-1} (δ Si-O(H)).

Surface-Initiated Ring Opening Polymerization of ε-caprolactone from SiO_2-GPS-OH NPs (SiO_2-GPS-PCL-OH NPs), 2

Dry SiO_2-GPS-OH (1.05 g) were crushed with mortar and pestle, then dispersed in ε-caprolactone (40 mL, 0.361 mol) via sonication in a flame dried 50 mL, 2-neck round bottom flask equipped with a PTFE stir bar under positive nitrogen pressure for 20 minutes. TBD (0.11 g, 0.76 mmol) was added, then reacted for ~3 h under nitrogen gas. After 3 h, an excess of THF was added to dilute the reaction. Five cycles of centrifuge washes were completed with THF as the solvent, dispersing the nanoparticles with a vortexer each time. The supernatant was collected at each step and concentrated via rotary evaporation for precipitation in a 600 mL beaker, containing a 50:50 by volume mixture of cold hexanes and diethyl ether, followed by vacuum filtration. The nanoparticles were then dried at room temperature under high vacuum overnight (14 h). The reaction yielded 1.47 g of product at 62.25% yield calculated from TGA percent weight change from previous SiO_2-GPS-OH NPs. TGA: 35.89% (25-600˚C) increase by weight from previous SiO_2-GPS-OH NPs; FTIR: 3400-3000 cm^{-1} (ν O-H), 2944 cm^{-1} (ν_{as} C-H), 2864 cm^{-1} (ν_s C-H), 1723 cm^{-1} (ν C=O), 1500-1300 cm^{-1} (δ_s C-H), 1250-950 cm^{-1} (ν Si-O(Si)), 850-775 cm^{-1} (δ Si-O(H)).

Post Polymerization Functionalization of SiO_2-GPS-PCL-OH NPs with (2-bromo)isobutyryl bromide (SiO_2-GPS-PCL-Br NPs), 3

Dry SiO_2-GPS-PCL-OH (0.76 g) nanoparticles were weighed out and crushed with mortar and pestle before adding to a 100 mL, 2-neck round bottom flask equipped with a PTFE stir bar. Dimethylformamide (DMF, 90 mL, 1.16 mol) was added to disperse the nanoparticles. This stirred at room temperature under positive nitrogen gas atmosphere for 30 min. The reaction was then cooled down with ice for 10 min followed with the addition of pyridine (18 mL, 0.22 mol). Once chilled, BiBB (7.5 mL, 0.06 mol) was added dropwise via syringe into the reaction flask at high stirring (450 RPM). When all the BiBB was added, the reaction mixture was allowed to warm to room temperature and react overnight (14 h). It must be noted that while the reaction time was 14 h, most of the reaction takes place within the first 15-30 min and is continued for quantitative coupling. After 14 h, the solution was quenched with excess DMF and slowly poured into a 500 mL beaker containing 250 mL of saturated sodium bicarbonate solution. Centrifuge/wash cycles consist of three times with THF, three times with THF/aqueous sodium bicarbonate ($NaHCO_3$ aq) (50:50), and five times with DIW. The supernatant was decanted off at each step and after the final step the product was dried under high vacuum at 25 ˚C overnight (14 h). For the final product, 0.64 g of material was collected at 99.14% yield calculated from TGA percent weight change from the previous SiO_2-GPS-PCL-OH NPs. TGA: 0.51% (25-600˚C) by weight increase from previous step SiO_2-GPS-PCL; FTIR: 3400-3000 cm^{-1} (ν O-H), 2945 cm^{-1} (ν_{as} C-H), 2864 cm^{-1} (ν_s C-H), 1723 cm^{-1} (ν C=O), 1500-1300 cm^{-1} (δ_s C-H), 1250-950 cm^{-1} (ν Si-O(Si)), 850-775 cm^{-1} (δ Si-O(H)).

Surface-Initiated ATRP of Oligo(ethylene glycol)methyl methacrylate mono-methyl ether (OEGMA) from SiO_2-GPS-PCL-Br NPs (SiO_2-GPS-PCL-POEGMA-Br NPs), 4

OEGMA (19.5 mL, 0.04 mol), dry SiO_2-GPS-PCL-Br (0.2 g) nanoparticles, Me_6TREN (0.1 mL, 0.37 mmol), and toluene (5 mL, 0.05 mol) were added to a 100 mL, 2-neck round bottom flask with a PTFE stir bar and stirred for 15 min under positive nitrogen gas flow. Additionally, EBiB (0.03 mL, 0.2 mmol) was added for the purpose of sacrificial free initiator. Three freeze-pump-thaw cycles were performed on the reaction mixture to remove air and water. Cu(I)Br (0.04 g, 0.27 mmol) was added to the frozen solution before the last freeze-pump-thaw cycle. The flask was then allowed to warm to room temperature and react for 3 hrs under inert nitrogen gas atmosphere. The reaction was quenched via exposure to air and diluted with excess toluene. The reaction was worked up via several centrifuge wash cycles comprising of three times with toluene, three times with 50:50 toluene/aqueous ammonium chloride (NH_4Cl aq), two times with methanol, and three times with deionized water. The samples were left dispersed in deionized water for long term storage. The yield was 0.17 g. Based on percent weight change collected from TGA, the yield was 52.68%. TGA 27.77% (25-600˚C) by weight increase from previous SiO_2-GPS-PCL-Br NPs; FTIR: 3400-3000 cm^{-1} (ν O-H), 2944 cm^{-1} (ν_{as} C-H), 2866 cm^{-1} (ν_s C-H), 1723 cm^{-1} (ν C=O), 1500-1300 cm^{-1} (δ_s C-H), 1250-950 cm^{-1} (ν Si-O(Si)), 850-775 cm^{-1} (δ Si-O(H)).

Functionalization of SiO_2-GPS-OH NPs with (2-bromo)isobutyryl bromide (SiO_2-GPS-Br NPs), 5

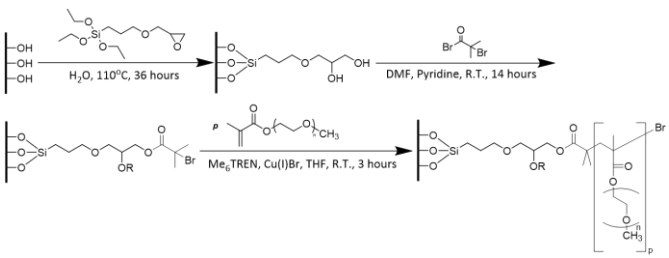

Scheme 2: Synthesis of SiO_2-GPS-POEGMA-Br nanoparticles

SiO_2-GPS-Br nanoparticles were prepared using the protocol from the synthesis of 3 (SiO_2-GPS-PCL-Br nanoparticles) above. Dry SiO_2-GPS-OH (1.01 g), (125 mL, 1.61 mol), pyridine (12.5 mL, 0.16 mol), and BiBB (10 mL, 0.08 mol) were added to the reaction. The yield was 0.83 g of SiO_2-GPS-Br NPs. Based on percent weight change collected from TGA, the yield was 98.78%. TGA 2.1% (25-600˚C) by weight increase from previous SiO_2-OH NPs.

Surface-Initiated ATRP of Oligo(ethylene glycol)methyl methacrylate mono-methyl ether (OEGMA) from SiO_2-GPS-Br NPs (SiO_2-GPS-POEGMA-Br NPs), 6

SiO_2-GPS-POEGMA-Br nanoparticles were prepared using the protocol from 4 (SiO_2-GPS-PCL-POEGMA-Br nanoparticles) above. OEGMA (20 mL, 0.04 mol), dry SiO_2-GPS-Br (0.21 g) nanoparticles, Me_6TREN (0.1 mL, 0.37 mmol), EBiB (0.05 mL, 0.34 mmol), Cu(I)Br (0.04 g, 0.31 mmol), and toluene (5 mL, 0.05 mol) were added to the reaction. The yield was 0.19 g. Based on percent weight change collected from TGA, the yield was 53.67%. TGA 47.46% (25-600˚C) by weight increase from previous SiO_2-GPS-Br NPs.

Thermogravimetric Analysis (TGA): Measurements were taken on a Thermo Scientific Q500. All data were collected from a tared 100 µL platinum sample pan. The dry sample protocol consisted of ramping the temperature from 25˚C to 600˚C at a rate of 5 ˚C min^{-1} under inert nitrogen atmosphere (flow rate 10 mL min^{-1}), followed by an isothermal hold at 600 ˚C for 30 min. For the case of the nanoparticles dispersed in deionized water, and those that have been dispersed in deionized water exposed to oil, samples were ramped in temperature at a rate of 5˚C min^{-1} from 25˚C to 100˚C in inert nitrogen atmosphere (flow rate 10 mL min^{-1}) and held at 100˚C for 5 min isothermally to remove all water presence. Following the removal of water, measurements were collected from 100˚C to 500˚C at a ramp rate 10˚C min^{-1} in an air (flow rate 10 mL min^{-1}) atmosphere. Measurements are presented in the form of weight percent as a function of temperature (˚C).

Nuclear Magnetic Resonance (NMR): Measurements, proton (^1H) and carbon (^{13}C), were collected on a Bruker Avance 300 MHz instrument. Deuterated chloroform ($CDCl_3$) was used for the free, un-grafted PCL samples and deuterated methanol (MeOD-d_4) was used for the free, un-grafted POEGMA samples. In the case of the surface cleaved PCL-b-POEGMA copolymers measurements were collected in deuterated dimethylsulfoxide (DMSO-d_6). Samples for ^1H NMR measurements were prepared at a concentration of 10 mg mL^{-1} with a sufficient number of scans taken at 5 sec of relaxation time and 298K to achieve acceptable signal to noise. Samples for ^{13}C NMR measurements prepared at a concentration of 50 mg mL^{-1} with a sufficient number of scans taken at 5 sec of relaxation time and 298K to achieve acceptable signal to noise.

Gel permeation chromatography (GPC): Data were collected with a Waters 1515 isocratic high-performance liquid chromatography (HPLC) pump, and Waters 2414 refractive index (RI) detector with three Polymer Standard Service (PSS) styrene/divinylbenzene (SDV) analytical 500 Å (8 x 300 mm) columns in series (Polymer Laboratories Inc.). Runs were performed with an injection load of 50 µL for 45 min at 1 mL min^{-1} purge flow rate. Samples were made up at a concentration of 4 mg mL^{-1} in tetrahydrofuran (THF) and filtered through a Whatman 0.45 µm filter. The unit was heated to an internal temperature of 30˚C with a sampling interval of 2 measurements sec^{-1}. Measurements are presented in the form of mV, from the RI detector, with respect to retention time in minutes. Molecular weight and dispersity measurements were calculated from comparison against poly(styrene) standards.

Fourier Transform Infrared Spectroscopy (FTIR): Spectra were collected on a Thermo Nicholet NEXUS 670 FTIR. Samples were made up into potassium bromide (KBr) pellets at a concentration of 5 mg of sample per 100 mg of KBr. The mixture was ground via mortar and pestle and dried under high vacuum for 10 minutes before manually pressing into a pellet. A background consisting of 32 scans of ambient air was

collected immediately prior to each sample. Samples were placed in an inert nitrogen chamber and allowed to equilibrate for 5 minutes before collecting measurements. Measurements were collected in absorbance over 64 scans, resolution of 1 cm^{-1}, and data spacing of 0.482 cm^{-1}. Data is presented in the form of wavenumbers (cm^{-1}) to absorbance intensity from 400 to 4000 cm^{-1} wavenumbers.

Transmission Electron Microscopy (TEM): Images were collected on a FEI TECNAI G2F30 instrument. Both room temperature & cryogenic TEM experiments were performed for the following study at 200 kV. Cryogenic TEM samples were made up at a concentration of 1.5 mg mL^{-1} in deionized water. Utilizing a FEI Vitrobot, 5 µL of sample on a lacey carbon 200 mesh copper TEM grid and then the grid was plunged into liquid ethane after being sufficiently blotted once by filter paper for 1.5 sec at 100% humidity. After samples were vitrified, they were transferred to and held at -170˚C in a cryogenic TEM holder. Room temperature TEM samples were made up at a concentration of 1 mg mL^{-1} in ethanol and sonicated until dispersed. Solutions were spotted on Formvar carbon film supported, 200 mesh, square pore copper TEM grids. The grids dried ambiently before being inserted into the TEM instrument.

Dynamic light scattering (DLS): Analysis was performed on an ALV/ (CGS-3) four-angle, compact goniometer system (Langen, Germany), which consisted of a 22 mW HeNe linear polarized laser operating at a wavelength of λ = 632.8 nm and scattering angles from θ = 30-150°. Fluctuations in the scattering intensity were measured via an ALV LSE-5004 multiple tau digital correlator and analyzed via the intensity autocorrelation function ($g^{(2)}\tau$). Decay rates, Γ, were obtained from single-exponential fits using a second-order cumulant analysis, and the mutual diffusion coefficient, D_m, was calculated through the relation: $\Gamma = D_m q^2$, where q^2 is the scalar magnitude of the scattering vector. The hydrodynamic radius (R_h) was calculated through the Stokes-Einstein equation:

$$D_m \approx D_o = \frac{k_B T}{6\pi\eta_s R_h}$$

where D_m is approximately equal to the self-diffusion coefficient, D_o, k_B is the Boltzmann constant, T is the absolute temperature, and η_s is the solvent viscosity. For a plot of the decay rate of the intensity autocorrelation function vs. q^2, the diffusion coefficient is given by the slope, with the intercept passing through the origin. From this, the hydrodynamic radius (R_h) is determined. The brush thicknesses can be determined by subtracting the bare nanoparticle radius (75 nm) from the radius of the polymer-modified nanoparticle. Light scattering measurements were performed at 25 °C. Samples were diluted to 1 mg mL^{-1} (0.1 wt. %) in water or THF and passed through a 0.45 µm poly(ether sulfone) or poly(vinylidene fluoride) syringe filter into a pre-cleaned, borosilicate test tube for analysis.

Differential Scanning Calorimetry (DSC): Analysis was performed on a TA Instruments Q200 DSC by ramping from ambient to 100 °C under ultra-high purity (UHP) nitrogen flowing at 50 mL min^{-1} followed by a 5-minute isothermal hold to remove residual water from the sample. After the hold, the sample purge gas was switched to dry house air flowing at 50 mL min^{-1} and the sample was ramped at 10 °C min^{-1} to 500 °C. Quantification of the oil present was performed by integrating the area of the oxidation exotherm occurring from approximately 280-420 °C from samples exposed to British Petroleum (BP) crude oil and 180-420 °C for samples exposed to crude oil obtained from the Anadarko Petroleum Corporation. Both BP and Anadarko crude oil had previously been analysed in triplicate by the same DSC method to yield the reference exotherms for quantitation. DSC analysis of the nanoparticles that had not been exposed to crude oil was also performed to examine any potential exothermic peaks which would interfere with the analysis of crude oil uptake.

The examination of crude oil uptake was performed by stirring a mixture of the nanoparticles suspended in deionized water (DIW) with an equal volume of crude oil. DSC analysis of oxidative exotherms due to entrapped oil in the aqueous nanoparticle phase were then used to quantify the amount of entrapped oil relative to the concentration of the suspended nanoparticles. The method used was as follows: The stirring was performed in a capped 0.5 dram vial using a 6 mm × 5 mm Pyrex™ stir bar. The total volume of nanoparticle suspension was 500 µL, vigorously stirred with 500 µL of crude oil. At prescribed time intervals, stirring was stopped and the samples stood undisturbed for 5 minutes to allow for phase separation of the aqueous and oil phases. Sampling of the aqueous nanoparticle phase was performed by removing 40 µL of the nanoparticle suspension via syringe. The initial 10 µL of sample was then discarded, the syringe needle gently wiped to remove residual oil, then 20 µL of sample was added to a tared high-volume aluminum DSC pan. The sample mass was recorded before DSC analysis.

Surface Tension (ST) Measurements: Surface tension was measured using the pendant drop technique on a standard goniometer (Rame'-Hart, model 250). This technique was modified from the work performed by Farinmade *et al*.[52] To track the drop in surface tension from SiO_2-GPS-PCL-POEGMA-Br nanoparticles, the nanoparticles were dispersed in de-ionized water at 0.2, 0.01, 0.005, 0.0025, 0.00175, 0.001, 0.0005, and 0.0001 mg mL^{-1}. All of the nanoparticle suspensions were compared against a de-ionized water control. Thirty µL of the suspension containing nanoparticles was drawn from the vial with a flat tip needle by an automatic Rame'-Hart dispenser. Eleven µL of the suspension was ejected from the needle and measurements were collected once per three seconds, for 100 measurements. Drop shape analysis (DROPimage Advanced software) was used to determine the change in water surface tension over time. All control experiments were done using the same procedures.

Results and discussion

Synthesis and Characterization of SiO_2NP-GPS-PCL-POEGMA Copolymer Grafted Nanoparticles

Amphiphilic grafted nanoparticles were synthesized primarily focusing on the concept of simple "mix and react" chemistries. These poly(caprolactone)-*block*-poly[oligo(ethylene glycol) methyl methacrylate mono methyl ether] (PCL-*b*-POEGMA) SiO_2 NPs utilize architectural design and a tuned ratio of polymer content. Specifically targeting a ratio of linear hydrophobic polymers, facilitating oil encapsulation, to branched hydrophilic polymers allowing dispersibility in an aqueous environment. Polymerization protocols to synthesize these nanoparticle systems were chosen such that scale up would be more suitable than previous routes.[1,4–6] For example, SI-ROP grafting ε-caprolactone from the attached GPS utilized a guanidine base, TBD,[44] as a room temperature catalyst following the work of Simón et al., in contrast to using tin(II) 2-ethylhexanoate[36] which requires temperatures of 130˚C and longer reaction times. Modifications were also made to the previous work by Wu et al. to achieve sufficient POEGMA attachment to the

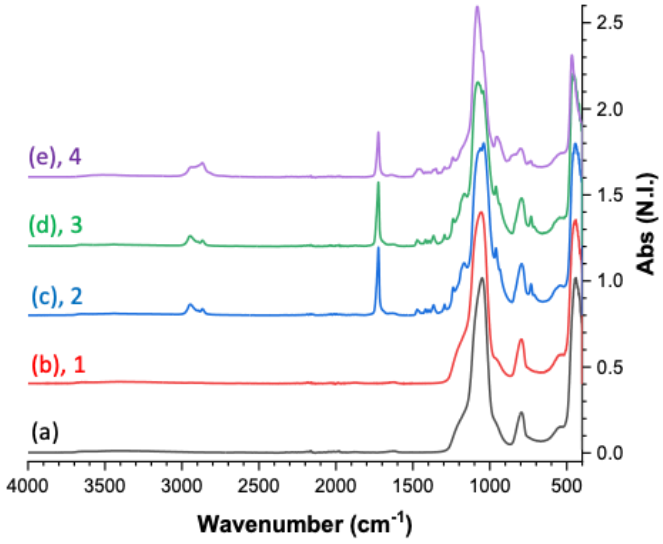

Figure 2: ATR-FTIR spectra of a) bare SiO_2-OH nanoparticles, b) SiO_2-GPS-OH (1), c) SiO_2-GPS-PCL-OH (2), d) SiO_2-GPS-PCL-Br (3), e) SiO_2-GPS-PCL-POEGMA-Br (4)

ATRP modified PCL chains.[30]

Following Scheme 1, functionalization of the bare SiO_2 NPs with (3-glycidoxypropyl)triethoxysilane (GPS), 1, produces consistent results to the literature[5] with the nanoparticles still dispersible in deionized water. FTIR measurements of SiO_2-GPS-PCL-OH NPs (Figure 2) depicts successful PCL grafting with the presence of increased alkyl stretching (2864 cm^{-1} ν_s C-H, 2944 cm^{-1} ν_{as} C-H, 1300-1500 cm^{-1} δ_s C-H) and increased carbonyl stretching (1723 cm^{-1} ν C=O) relative to the previous SiO_2-GPS-OH NPs. The asymmetric aliphatic stretching is approximately two to three times higher than the symmetric aliphatic stretching, consistent with literature findings for PCL polymers.[37] Polymer presence lends to reduced hydroxyl (3000-3400 cm^{-1} ν O-H) and silica (950-1250 cm^{-1} ν Si-O(Si), 775-850 cm^{-1} δ Si-O(H)) functionality overall. The SiO_2-GPS-PCL-OH nanoparticle samples, prepared via TBD catalyst, were found to be readily dispersible in organic solvents (THF) and lack solubility in water, in contrast to the precursor SiO_2-GPS-OH nanoparticles from the last step. FTIR observations of ATRP functionalized grafted PCL chains, SiO_2-GPS-PCL-Br NPs, appear identical to the previous SiO_2-GPS-PCL-OH NPs. The attachment of multiple oligo(ethylene glycol)methyl methacrylate mono-methyl ether (OEGMA) monomers from grafted PCL functionalized with an ATRP initiator was qualitatively confirmed by the ability to disperse the nanoparticles in DIW for an extended period of time (~2 hr). Reactions with low conversion of OEGMA, or no conversion at all, would remain dispersible in only organic solvents.

For the purposes of this study an M_n = 500 Da OEGMA monomer was utilized, with approximately nine ethylene glycol units in the side chain. The size of the oligo(ethylene glycol) side chains lends to increased symmetric (2866 cm^{-1} ν_s C-H) alkyl stretching, with a slight broadening in carbonyl stretching (1723 cm^{-1} ν C=O) seen in Figure 2. While the carbonyl stretch appears smaller in intensity than the previous step, it is in fact increased overall due to the presence of the carbonyls on the methacrylate backbone of the POEGMA polymer block. The overlap of the two carbonyls causes this

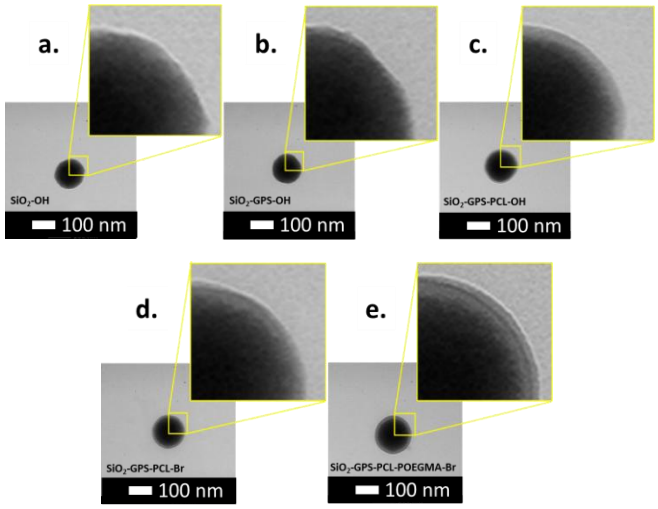

Figure 3: Room temperature TEM images (scale = 100 nm): a) SiO_2-OH, b) SiO_2-GPS-OH (1), c) SiO_2-GPS-PCL-OH (2a), d) SiO_2-GPS-PCL-Br (3a), e) SiO_2-GPS-PCL-POEGMA-Br NPs (4a)

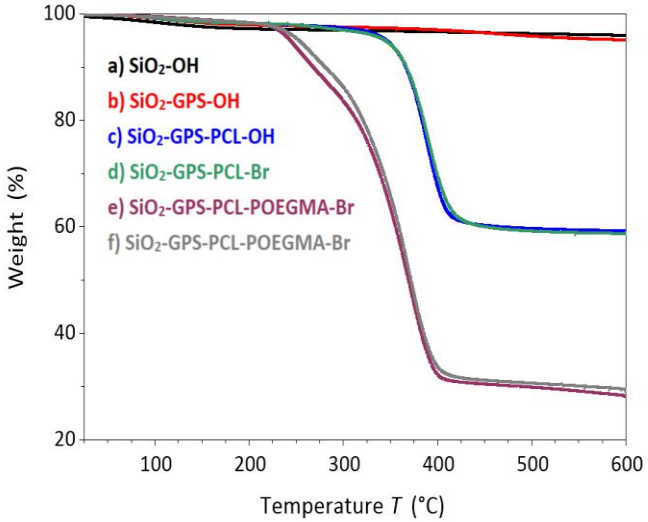

Figure 4: TGA spectra illustrating the synthetic progression of sample 4a from: a) bare SiO_2-OH nanoparticles, b) SiO_2-GPS-OH, c) SiO_2-GPS-PCL-OH, d) SiO_2-GPS-PCL-Br, e) SiO_2-GPS-PCL-POEGMA-Br, and f) SiO_2-GPS-PCL-POEGMA-Br after redispersion in water from dry storage conditions.

slight broadening of the peak shown in Figure 2. Further, greatly increased symmetric stretching (2866 cm^{-1} ν_s C-H) from the ethylene glycol side-chains, as well as the increase of the C-O character at approximately 1100 cm^{-1}, reinforces the presence of POEGMA on the NPs.[53]

Tracking the reactions (sample 4a) from start to finish using room temperature TEM imaging (Figure 3) without solvent clearly shows a growing polymer corona on the surface of the dry NPs. Comparing Figure 3(a) (SiO_2-OH NPs) to Figure 3(b) (SiO_2-GPS-OH NPs) sets the baseline for both at 65±2 nm in radius. Functionalization with GPS (sample 1) did not significantly increase the corona, consistent with FTIR (Figure 2) measurements. Once PCL is successfully grafted (sample 2a) from the surface of these SiO_2-GPS-OH NPs, a clear polymer corona is shown in Figure 3(c) with a brush thickness of ~10 nm taken from the total radius of 75±2 nm (SiO_2-GPS-PCL-OH NPs). This size is not appreciably increased in Figure 3(d) when SiO_2-GPS-PCL-OH is functionalized with BiBB (sample 3a) via post-polymerization reaction, again consistent with FTIR (Figure 2) measurements. Addition of the second block, POEGMA (sample 4a), via SI-ATRP increases the brush thickness to ~15 nm, a difference of ~5 nm, taken from a total NP radius of 80±2 nm. Additionally, two layers can be seen upon closer inspection of Figure 3(e) due to the contrast in electron densities apparent from the core-shell structure. Figure 3(e) depicts a darker interstitial space between the PCL and POEGMA and adjusting the contrast had no effect on the appearance overall.

Table 1: Percent (%) polymer values calculated from TGA measurements.

Sample	*2a*	*4a*	*4b*	*4c*	*4d*	*6*
% PCL	37	20	8	25	12	0
% POEGMA	0	46	61	33	43	45
% SiO_2 NP	63	34	31	42	45	55

Quantitative confirmation of the synthesis was observed via increased mass loss in percent by weight measured on a TGA instrument, complimenting FTIR (Figure 2) and TEM (Figure 3) observations above. When comparing SiO_2-GPS-OH NPs and the bare SiO_2-OH NPs (Figure 4) via TGA measurements, only a 2% increase in mass loss was observed in the former. The surface functionalization of the NP cores with GPS was determined to be a necessary step and remains the only step in the total synthesis requiring elevated temperature of 110°C. While there was a minimal addition of mass from the initiator, the effective increase of the hydroxy content on the surface provides grafting points for the surface-initiated ring opening polymerization (SI-ROP) of ε-caprolactone in the second reaction step. It will be noted that the grafting of ε-caprolactone was attempted directly from the bare SiO_2-OH NP surface with no success, with either the tin(II) 2-ethylhexanoate[36] catalyst or the 1,5,7-triazabicyclo[4.4.0]dec-5-ene (TBD)[43] catalyst. The tin(II) 2-ethylhexanoate protocol was attempted at 130˚C, resulting in low overall percent by weight mass loss of PCL on the surface of the NPs (data not shown). However, using the room temperature TBD catalyst protocol, PCL was grafted from the surface of the nanoparticle with an observed increased mass loss (Figure 4, Table 1) of 37% by weight (sample 2a, 375 to 425˚C), with the remaining 63% being the SiO_2 NP core and attached GPS. Repetitive SI-ROP reactions were required with the tin(II) 2-ethylhexanoate catalyst. Linear ungrafted PCL (M_n 10 kDa) was measured via TGA as a reference for the above spectra to confirm that the degradation event occurring from 375 to 425˚C (Figure S8) was from PCL. Repeat SI-ROP reactions generated mass losses of 21% PCL (sample 2b), 37% PCL (sample 2c), and 22% PCL (sample 2d) by weight. TGA mass losses appreciably represent comparable conversion of polymer on the surface of the nanoparticles. After confirmation of successful PCL grafting, surface-grafted PCL chains were functionalized with (2-bromo)isobutyryl bromide (BiBB) with an observed increased mass loss (less than 1% by weight, Figure 4) from the previous SiO_2-GPS-PCL-OH NPs. While there was increased added mass from the ATRP initiator, this step provides means to set up chain extension of surface-grafted PCL via the ATRP of OEGMA monomer. The extent of POEGMA surface grafting was quantified by the increased percent by weight mass loss (Figure 4, Table 1) from 37% (sample 2a, 375 to 425˚C, 60% SiO_2 NP core) to 66% polymer (sample 4a, 225 to 425˚C, 31% SiO_2 NP core). Repeat samples 4b, 4c, and 4d had percent by weight mass losses (Table 1) of 69%, 58%, and 55% polymer respectively. This percentage was confirmed by collecting TGA measurements of ungrafted (M_n 14 kDa) POEGMA (275 to 350˚C, Figure S8) and referencing the previous ungrafted PCL (375 to 425°C, Figure S8). Having greater than fifty percent total grafted copolymer content of the NPs, the exterior POEGMA tends to dominate polymer derived structure-property relationships aiding in increased oil encapsulation and sustained dispersion in water.

Tailoring Co-polymer Block Length to Increase Oil Encapsulation & Dispersibility in Water

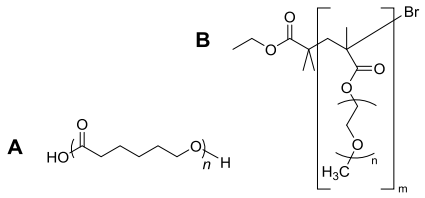

Chart 1: The structure of water-initiated PCL (A, left), and the structure of EBiB-initiated POEGMA (B, right)

In order to gain a better knowledge of the structure-property relationships, the relative size and number of grafted polymers on the surface of the nanoparticles needed to be quantified. Given the same stock nanoparticles, following conversion of the products throughout the reactions shows increased or decreased water dispersibility based on the ratio between the hydrophilic (POEGMA) and hydrophobic (PCL) polymer blocks. This ratio was tracked through a series of reaction conditions to achieve systems with more hydrophobic character or hydrophilic character (Table 1). Additionally, pure hydrophobic PCL (sample 2a) or pure hydrophilic POEGMA (sample 6) were also included.

Table 2: Number-average molecular weights calculated from NMR and GPC traces of ungrafted polymers with calculated repeat units (R.U.)

Sample	*2a*	*4a*	*4b*	*4c*	*4d*	*6*
NMR $M_{n\ PCL}$	2600	2600	1000	2600	1200	0
NMR R.U. $_{PCL}$	22.6	22.6	8.6	22.6	10.4	-
GPC $M_{n\ PCL}$ (PS cal values)	6100	6100	2300	6100	2600	0
GPC $M_{n\ PCL}$ (adjusted values)	3000	3000	1000	3000	1200	-
GPC R.U. $_{PCL}$ (adjusted values)	26.4	26.4	8.6	26.4	10.4	-
GPC M_n POEGMA	0	14200	13700	11000	10900	13300
GPC R.U. POEGMA	-	28.0	27.0	21.6	21.4	26.2

The addition of free initiator was first considered, as this allowed the polymerization of ungrafted "free" polymer in situ.[5] Adventitious water, liberated from the surface of the SiO_2 NPs,[2] provided adequate initiation during the SIROP reaction to generate water-initiated PCL, in situ, that was ungrafted from the nanoparticle. This ungrafted polymer was analyzed via NMR to confirm the structure, and the approximate molecular weight of the grafted chains was confirmed via GPC. Proton (^{1}H, Figure S13-15) and carbon (^{13}C, Figure S16) NMR spectra were collected in deuterated chloroform to confirm the structure of ungrafted PCL (Chart 1-A) initiated from adventitious water during the SI-ROP reaction. As adventitious initiator was not present during the SI-ATRP, ethyl 2-bromoisobutyrate (EBiB) was utilized as the initiator to generate free POEGMA in solution. The structure of EBiB-initiated POEGMA (Chart 1-B) generated during the SI-ATRP reaction was confirmed by ^{1}H (Figure S21-25) and ^{13}C NMR (Figure S26) in deuterated methanol.[54–57] PCL-b-POEGMA copolymers were not generated in situ as all free PCL polymer from the SI-ROP reaction was removed during the workup.

While confirmation of the structures is useful to clarify success of the reactions, the structure-property relationships are also drawn from the molecular weight of the grafted polymers. The overall ratio of hydrophobic polymer vs. hydrophilic polymer balances the ability to enhance oil encapsulation with sustained water dispersibility. Therefore, it was ultimately necessary to track the size of the polymers on the surface both from molecular weight measurements and from relative size in solution. Because POEGMA is a bulky bottlebrush polymer with each monomer unit weighing approximately 500 Da, it tends to increase water dispersibility with fewer repeat units per polymer chain. Linear PCL, with a monomer molecular weight of 114 Da, is swellable as oil becomes encapsulated, with an uptake capacity that is expected to increase with increasing degree of polymerization. In order to design a system accounting for both desired properties, GPC measurements of ungrafted polymer were tracked over a series of reactions to monitor molecular weight (Table 2). Samples were chosen to reflect varying ratios between the hydrophobic and hydrophilic polymers, as well as their ability to encapsulate crude oil. As hypothesized, the nanoparticle systems containing only PCL (sample 2) and no POEGMA could be dispersed in an oil layer but had no ability to be used in aqueous setting to take up oil. On the other hand, samples containing all POEGMA (sample 6) and no PCL could be easily dispersed in aqueous environments but had no ability to take up oil.

Ungrafted polymers are commonly utilized to approximate the molecular weights of their grafted counterparts.[5] Therefore, the M_n value of ungrafted PCL, established by both NMR and GPC measurements in Table 2, could be utilized alongside the percent polymer compositions in Table 1 to approximate the M_n of grafted POEGMA. Following this, 3 kDa grafted PCL present on sample 4a would imply that grafted POEGMA would have an M_n of approximately 6.9 kDa. While this would be indicative of a much larger POEGMA chain, it must be considered that the repeat unit of POEGMA is roughly five times the mass of the caprolactone repeat unit of PCL. In the case of sample 4a, the copolymer chain would have 26 repeat units of ε-caprolactone monomer for every 14 repeat units of OEGMA monomer. Ignoring the presence of side chains for a moment, a strictly linear backbone would contain a PCL chain contour length of approximately 27 nm, and a POEGMA chain length of 4 nm. As such, the higher number of caprolactone units to OEGMA units contributed to structure-property relationships of oil encapsulation while still maintaining dispersion in water. This concept can be applied to samples 4b-d in order to further reaffirm these hypotheses.

Sample 4b maintains 1 kDa grafted PCL, approximating the grafted POEGMA to an M_n of 7.6 kDa. When this is simplified in

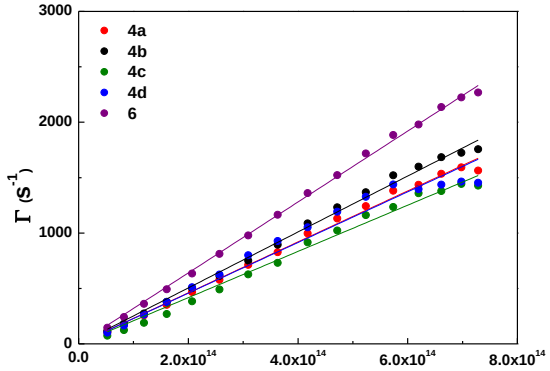

Figure 5: DLS measurements in THF illustrating the size of several SiO_2-GPS-PCL-POEGMA-Br NPs (sample 4a-d) and SiO_2-GPS-POEGMA-Br NPs (sample 6)

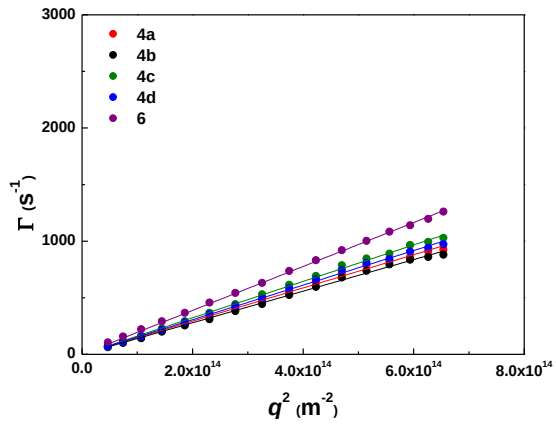

Figure 6: DLS measurements in deionized water illustrating the size of several SiO_2-GPS-PCL-POEGMA-Br NPs (sample 4a-d) and SiO_2-GPS-POEGMA-Br NPs

terms of repeat units, 8 ε-caprolactone units are present with 15 OEGMA units. Considering a strictly linear chain once again, this equates to a linear PCL chain contour length of approximately 8 nm and a POEGMA backbone length of 4 nm. Sample 4c represents the minimum ratio of 3 kDa PCL to approximately 4 kDa POEGMA, 26 ε-caprolactone units for every 8 OEGMA units, in order to maintain dispersion in water but still possess the ability to uptake oil. In terms of approximate length this represents a PCL chain contour length of 27 nm with a POEGMA chain length of 2 nm. It will be noted that sample 4c did not perform as well as sample 4a in terms of the end goal application. This is thought to arise from the increased POEGMA molecular weight of sample 4a lending to increased stability in the aqueous phase with minimal energy input. While sample 4c did appear to encapsulate a minute amount of oil, it could not maintain suspension in water for extended periods successfully. Sample 4d, much like sample 4b, did not encapsulate oil with an approximated grafted 1.2 kDa PCL and 4.3 kDa grafted POEGMA. This corresponding to 10 ε-caprolactone repeat units to every 9 OEGMA units respectively, resembling a ratio of almost equal part PCL to POEGMA. Both sample 4b and 4d were dispersible in aqueous conditions. Because sample 4d possessed an approximate PCL chain contour length of 10 nm and POEGMA chain length of approximately 2.7 nm, it did not maintain suspension for extended periods of time.

As previously mentioned, the SiO_2-GPS-PCL-POEGMA-Br (samples 4a-d) and SiO_2-GPS-POEGMA-Br (sample 6) nanoparticles dispersed into water; however, the nanoparticles did not disperse as well in THF based on visual inspection of the clarified solutions. This is thought to be due to the slight incompatibility of POEGMA with THF. Despite this, DLS measurements in THF were able to be taken, and a larger nanoparticle size compared to water was observed. These DLS observations (Figure 5 and 6) show an increase in hydrodynamic radius (R_h) when the samples are in THF. This correlates with expected results, as THF is a good solvent for PCL and an adequate solvent for POEGMA. Once the samples are placed in water, the hydrophobic, PCL, block collapses, and R_h exhibits a corresponding decrease in radius.

Sample	*4a*	*4b*	*4c*	*4d*	*6*
R_h *(THF, nm)*	208	190	230	209	150
R_h *(H_2O, nm)*	166	175	151	160	126
Δ (nm)	42	15	79	49	24

Table 3: Comparing sample size of SiO_2-GPS-PCL-POEGMA-Br NPs by DLS measurement in THF & DIW

These samples had a relatively narrow dispersity in the size distribution in water (PDI ~ 0.1 from second order cumulant analysis). In contrast, the dispersity increased for measurements in THF, although they still remained relatively monodisperse (PDI ~0.1 – 0.3). This observation is seen due to two reasons: First, in THF, the disperse PCL chains are able to contribute to the PDI, whereas in water, the PCL block collapses to the surface of the nanoparticle due to solvent incompatibility and does not contribute to the PDI. Second, the POEGMA block displayed slight incompatibility with THF, which contributes to an increased PDI.

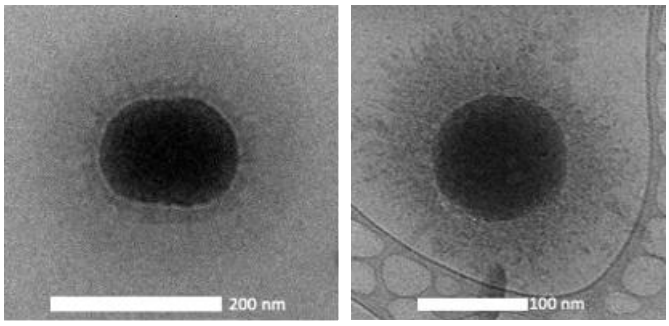

Figure 7: Cryo-TEM of SiO_2-GPS-PCL-POEGMA-Br NP (left, 4a), and SiO_2-GPS-PCL-POEGMA-Br after being stirred at a 1:1 ratio with BP crude oil for 72 hrs and allowed to settle for 5 days (right, 4a)

Analysis of measured oil uptake

Cryo-TEM imaging appears much like the room temperature TEM imaging (Figure 4), although the functionalized nanoparticles are representative to their natural state due to the presence of deionized water. Cryo-TEM imaging (Figure 7) of the final SiO_2-GPS-PCL-POEGMA-Br NPs (sample 4a) shows a polymeric density transition from the ~65±2 nm SiO_2 NP core radius to the ~25±2 nm inner hydrophobic PCL layer and finally the ~55±2 nm outer hydrophilic POEGMA layer. The PCL chains are collapsed upon themselves in an aqueous system making them appear denser or darker in color on the cryo-TEM image. When comparing

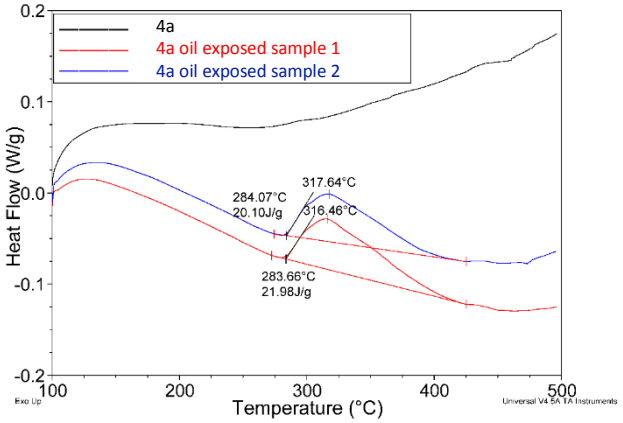

Figure 8: DSC exotherms of SiO_2-GPS-PCL-POEGMA-Br nanoparticle before BP crude oil exposure (sample 4a) and repeat samples following exposure for 72 hours (BP crude oil exposed sample 4a - 1, 2).

the nanoparticles, cryo-TEM imaging of SiO_2-GPS-PCL-POEGMA-Br NPs after exposure to BP crude oil indicates a much darker total corona around the nanoparticle core. No changes made to imaging contrast had any effect on this darker region. This behavior is suggestive of encapsulated oil microdroplets but needed to be confirmed by alternate techniques to quantify approximately how much oil was encapsulated.

DSC was used to quantify the potential oil uptake (Figures 8, S41-46) of four nanoparticle formulations (samples 4a-d), ranging in concentration from 3-5 mg mL^{-1}. The nanoparticles

in this initial study did not undergo any drying and redispersion steps following synthesis. Two of the formulations (samples 4b and 4d) showed no quantifiable oil exotherms while sample 4c showed very little appreciable oil exotherm. A fourth sample, 4a, showed a clear and readily quantifiable oil exotherm matching that of the oil reference sample. Repeat measurements of this sample taken at 72 hours showed an exothermic peak with an average integrated area of 21.04 ± 0.94 J g^{-1} of total sample (Figure 8). This corresponded to an approximately 9:1 fold uptake, by mass, of BP crude oil to nanoparticles in suspension.

Following the encouraging results of the oil exposure study, aliquots of sample 4a nanoparticles, which had undergone a drying and redispersion step following synthesis, were examined. The redispersion step for the samples consisted of either vigorous stirring by magnetic stir bar or sonication for 40 minutes. Redispersed samples were prepared at 3.7 mg mL^{-1}. Oil exposure for these nanoparticle samples was performed with Anadarko crude oil (Figure S33-34), as a means to demonstrate the broad application to a range of crude oil formulations. DSC analysis showed a marked difference between the dried samples redispersed by stirring and those redispersed by sonication. The sample redispersed by stirring showed no evidence of oil uptake at both 24- and 96-hour sampling timepoints, while the sonicated sample showed a 30-fold uptake at 24 hours (Figure S33) and 37-fold oil uptake at 96 hours (Figure S34).

As previously mentioned, Corexit™ has a measured CMC of approximately 22.5 mg L^{-1}.[8,11] Through surface tension measurements these amphiphilic grafted nanoparticles (AGNs) were found to have an apparent "CMC" of 2.62 mg L^{-1}. These nanoparticles exhibited a drop in surface tension (53.4 mN/m) from that of de-ionized water (70 mN/m) indicating that the nanoparticles are surface active and amphiphilic in nature. In comparison, the combined components of Corexit™ exhibit a drop in surface tension measured at approximately 30 mN/m, when above the CMC.[8] Though the presence of a "CMC" was noted for the SiO_2-GPS-PCL-POEGMA-Br nanoparticles, their usefulness as oil dispersants is not limited by this property, as confirmed by the reported DSC data. While the amphiphilic copolymer shell provides properties resembling self-assembled micelles, the covalent linkages ultimately prevent the polymers from disaggregation when below the "CMC" value. This is not to say that the assembly of AGNs does not disaggregate below the "CMC" as the mechanism is not fully understood. Further, the "CMC" of these nanoparticles is an order of magnitude lower than that of Corexit™ making them better suited to use in a large body of water. In future studies, the kinetics and mechanism of oil entrapment, and aquatic toxicity, similar to the work done by Kurita et al.,[58] will be investigated further. Thus, reinforcing the suitability of these polymer grafted nanoparticles as a replacement dispersant system for Corexit™ 9500.

Conclusions

PCL-*b*-POEGMA copolymers have been sequentially grafted from the surface of modified SiO_2 nanoparticles utilizing SI-ROP & SI-ATRP techniques. By utilizing well established chemistries, a primarily room temperature route has been completed for ease of scale up in an industrial setting. Through control of reaction times, PCL and POEGMA are easily tailorable to achieve desired molecular weights for the properties of high oil loading and sustained water dispersibility. The results of the initial oil uptake study show that a viable test method has been developed using DSC to quantify encapsulated oil. DSC revealed one of the developed nanoparticle formulations, specifically the sample with the least wt. % POEGMA to maintain dispersion, can entrap up to thirty times its own mass in crude oil within a 24-hr window. Future studies using this method for the analysis of oil uptake will be able to further refine the mechanism and kinetics of these nanoparticle formulations to entrap oil, especially in salinized and seawater environments. Further, future nanotoxicology studies of this system will determine the suitability in real-world applications involving aquatic organisms and species. The synthetic approach presented in this work provides the foundation for steering scientific research towards a better dispersant system.

Author Contributions

The author contributions, in order of authorship, are as follows. Christopher B. Keller's contributions are the primary synthesis and investigation, writing of the original draft, formal analysis of all datasets, methodology, validation, and visualization of the manuscript. Susan E. Walley's contributions are within the investigation, writing of the original draft, visualization, formal analysis, and validation of the DLS data. Dr. Curtis W. Jarand's contribution stems from the investigation, formal analysis, visualization, and validation of DSC data as well as the writing in the original draft associated with the DSC data. Dr. Jibao He's contribution stems from the investigation and validation of TEM data. Dr. Muhammad Ejaz's contribution concerns the early methodology as well as the validation of the current work. Dr. Daniel A. Savin's contribution lies in the conceptualization, funding acquisition, project administration, resources, supervision, and validation of the work. Dr. Scott M. Grayson's contribution also lies in the conceptualization, funding acquisition, project administration, resources, supervision, and validation of the work. All authors contributed to writing through reviewing and editing of the manuscript drafts.

Conflicts of interest

The authors hereby declare no conflicts of interest.

Acknowledgements

The authors acknowledge BP/Gulf of Mexico Research Initiative (RF-VI-G-231811) for funding. Data is made publicly

available through the Gulf of Mexico Research Initiative Information and Data Cooperative (GRIIDC) at https://data.gulfresearchinitiative.org (data sets R6.x827.000:0005, R6.x827.000:0006, and R6.x827.000:0007). The authors acknowledge NSF GRFP #1842473 for partial funding support of S.E.W. The authors acknowledge Nissan Chemical America Corporation for their donation of the Snowtex silica nanoparticles. The authors would like to acknowledge Azeem Farinmade in the John research group for assistance with collecting surface tension measurements. The authors also acknowledge the Shantz research group for use of their ATR-FTIR and TGA instruments, the Reed research group for use of their DSC instrument, and the Tulane University Coordinated Research Facility for use of the TEM instrument.

Corresponding author

Scott M. Grayson – Department of Chemistry, Tulane University, New Orleans, LA 70118, United States; orcid.org/0000-0001-6345-8762 Email: sgrayson@tulane.edu; Fax (+1) 504-865-5596

Notes and references

1 K. C. Bentz, M. Ejaz, S. Arencibia, N. Sultan, S. M. Grayson and D. A. Savin, *Polym. Chem.*, 2017, **8**, 5129–5138.
2 K. C. Bentz and D. A. Savin, *Macromolecules*, 2017, **50**, 5565–5573.
3 D. P. Norwood, E. Minatti and W. F. Reed, *Surfactant/Polymer Assemblies. 1. Surfactant Binding Properties*, 1998.
4 A. Pavía-Sanders, S. Zhang, J. A. Flores, J. E. Sanders, J. E. Raymond and K. L. Wooley, *ACS Nano*, 2013, **7**, 7552–7561.
5 M. Ejaz, A. M. Alb, K. A. Kosakowska and S. M. Grayson, *Polym. Chem.*, 2015, **6**, 7749–7757.
6 M. Ejaz, A. M. Alb and S. M. Grayson, *React. Funct. Polym.*, 2016, **102**, 39–46.
7 S. Li, X. Jiao and H. Yang, *Langmuir*, 2013, **29**, 1228–1237.
8 Z. Cai, Y. Gong, W. Liu, J. Fu, S. E. O'Reilly, X. Hao and D. Zhao, *Mar. Pollut. Bull.*, 2016, **109**, 49–54.
9 https://www.epa.gov/emergency-response/corexittm-ec9500a.
10 S. M. Techtmann, M. Zhuang, P. Campo, E. Holder, M. Elk, T. C. Hazen, R. Conmy, J. W. Santo Domingo, *Appl. Environ. Microbiol.*, 2017, **83**, 3462–3478.
11 Y. Gong, X. Zhao, S. E. O'Reilly, T. Qian and D. Zhao, *Environ. Pollut.*, 2014, **185**, 240–249.
12 G. Basu Ray, I. Chakraborty and S. P. Moulik, *J. Colloid Interface Sci.*, 2006, **294**, 248–254.
13 H. Liu, A. Jiang, J. Guo and K. E. Uhrich, *J. Polym. Sci. Part A Polym. Chem.*, 1999, **37**, 703–711.
14 T. Zhou, H. Qi, L. Han, D. Barbash and C. Y. Li, *Nat. Commun.*, 2016, **7**, 1–8.
15 C. Flesch, C. Delaite, P. Dumas, E. Bourgeat-Lami and E. Duguet, *J. Polym. Sci. Part A Polym. Chem.*, 2004, **42**, 6011–6020.
16 G. Bissadi and R. Weberskirch, *Polym. Chem.*, 2016, **7**, 1271–1280.
17 F. T. Oyerokun and R. A. Vaia, *Macromolecules*, 2012, **45**, 7649–7659.
18 M. K. Corbierre, N. S. Cameron and R. B. Lennox, *Langmuir*, 2004, **20**, 2867–2873.
19 C. Chevigny, D. Gigmes, D. Bertin, J. Jestin and F. Boué, *Soft Matter*, 2009, **5**, 3741–3753.
20 A. P. Martinez, J. M. Y. Carrillo, A. V. Dobrynin and D. H. Adamson, *Macromolecules*, 2016, **49**, 547–553.
21 C. J. Kim, K. Sondergeld, M. Mazurowski, M. Gallei, M. Rehahn, T. Spehr, H. Frielinghaus and B. Stühn, *Colloid Polym. Sci.*, 2013, **291**, 2087–2099.
22 J. Tom, K. Ohno and S. Perrier, *Polym. Chem.*, 2016, **7**, 6075–6083.
23 G. Carrot, D. Rutot-Houzé, A. Pottier, P. Degée, J. Hilborn and P. Dubois, *Macromolecules*, 2002, **35**, 8400–8404.
24 A. Sunder, M. Krämer, R. Hanselmann, R. Mülhaupt and H. Frey, *Angew. Chemie - Int. Ed.*, 1999, **38**, 3552–3555.
25 A. El Harrak, G. Carrot, J. Oberdisse, C. Eychenne-Baron and F. Boué, *Macromolecules*, 2004, **37**, 6376–6384.
26 M. Joubert, C. Delaite, E. Bourgeat-Lami and P. Dumas, *J. Polym. Sci. Part A Polym. Chem.*, 2004, **42**, 1976–1984.
27 T. von Werne and T. E. Patten, *J. Am. Chem. Soc.*, 2001, **123**, 7497–7505.
28 Y. Liu, V. Klep, B. Zdyrko and I. Luzinov, *Langmuir*, 2004, **20**, 6710–6718.
29 J. Pyun, T. Kowalewski and K. Matyjaszewski, *Macromol. Rapid Commun.*, 2003, **24**, 1043–1059.
30 L. Wu, U. Glebe and A. Böker, *Polym. Chem.*, 2015, **6**, 5143–5184.
31 C. M. R. Abreu, P. V. Mendoṇa, A. C. Serra, J. F. J. Coelho, A. V. Popov and T. Guliashvili, *Macromol. Chem. Phys.*, 2012, **213**, 1677–1687.
32 H. Ma, M. Wells, T. P. Beebe and A. Chilkoti, *Adv. Funct. Mater.*, 2006, **16**, 640–648.
33 P. F. Cañamero, J. L. De La Fuente, E. L. Madruga and M. Fernández-García, *Macromol. Chem. Phys.*, 2004, **205**, 2221–2228.
34 K. A. Davis, H. J. Paik and K. Matyjaszewski, *Macromolecules*, 1999, **32**, 1767–1776.
35 K. El Tahlawy and S. M. Hudson, *J. Appl. Polym. Sci.*, 2003, **89**, 901–912.
36 R. F. Storey and J. W. Sherman, *Macromolecules*, 2002, **35**, 1504–1512.
37 T. Elzein, M. Nasser-Eddine, C. Delaite, S. Bistac and P. Dumas, *J. Colloid Interface Sci.*, 2004, **273**, 381–387.
38 V. Rie Heroguez, Y. Gnanou and M. Fontanille, *Macromolecules*, 1997, **30**, 4791–4798.
39 R. K. Kainthan, C. Mugabe, H. M. Burt and D. E. Brooks, *Biomacromolecules*, 2008, **9**, 886–895.
40 C. Yang, S. Huang, X. Wang and M. Wang, *Polym. Chem.*, 2016, **7**, 7455–7468.
41 O. G. Schramm, G. M. Pavlov, H. P. Van Erp, M. A. R. Meier, R. Hoogenboom and U. S. Schubert, *Macromolecules*, 2009, **42**, 1808–1816.
42 P. Tambe, P. Kumar, K. M. Paknikar and V. Gajbhiye, *J.*

Control. Release, 2019, **299**, 64–89.

43 B. G. G. Lohmeijer, R. C. Pratt, F. Leibfarth, J. W. Logan, D. A. Long, A. P. Dove, F. Nederberg, J. Choi, C. Wade, R. M. Waymouth and J. L. Hedrick, *Macromolecules*, 2006, **39**, 8574–8583.

44 L. Simón and J. M. Goodman, *J. Org. Chem.*, 2007, **72**, 9656–9662.

45 W. Cao and L. Zhu, *Macromolecules*, 2011, **44**, 1500–1512.

46 A. El Harrak, G. Carrot, J. Oberdisse, J. Jestin and F. Boué, *Polymer (Guildf).*, 2005, **46**, 1095–1104.

47 G. Carrot, S. Diamanti, M. Manuszak, B. Charleux and J.-P. Vairon, *J. Polym. Sci. Part A Polym. Chem.*, 2001, **39**, 4294–4301.

48 A. B. Lowe, B. S. Sumerlin, M. S. Donovan and C. L. McCormick, *J. Am. Chem. Soc.*, 2002, **124**, 11562–11563.

49 H. Mori, D. C. Seng, M. Zhang and A. H. E. Müller, *Langmuir*, 2002, **18**, 3682–3693.

50 J. Pyun, S. Jia, T. Kowalewski, G. D. Patterson and K. Matyjaszewski, *Macromolecules*, 2003, **36**, 5094–5104.

51 M. Marini, M. Toselli, S. Borsacchi, G. Mollica, M. Geppi and F. Pilati, *J. Polym. Sci. Part A Polym. Chem.*, 2008, **46**, 1699–1709.

52 A. Farinmade, O. F. Ojo, J. Trout, J. He, V. John, D. A. Blake, Y. M. Lvov, D. Zhang, D. Nguyen and A. Bose, *ACS Appl. Mater. Interfaces*, 2020, **12**, 1840–1849.

53 S. Y. Chan, W. S. Choo, D. J. Young and X. J. Loh, *Polymers (Basel).*, 2016, **8**, 1–12.

54 L. Esser, N. P. Truong, B. Karagoz, B. A. Moffat, C. Boyer, J. F. Quinn, M. R. Whittaker and T. P. Davis, *Polym. Chem.*, 2016, **7**, 7325–7337.

55 G. Wang, M. Chen, S. Guo and A. Hu, *J. Polym. Sci. Part A Polym. Chem.*, 2014, **52**, 2684–2691.

56 R. Pires-Oliveira, J. Tang, A. M. Percebom, C. L. Petzhold, K. C. Tam and W. Loh, *Langmuir*, 2020, **36**, 15018–15029.

57 A. Skandalis and S. Pispas, *J. Polym. Sci. Part A Polym. Chem.*, 2017, **55**, 155–163.

58 H. Kurita, C. L. Brown, K. J. Kroll, S. E. Walley, C. Keller, M. Ejaz, M. Kozuch, W. Reed, S. Grayson, D. A. Savin and N. D. Denslow, *Aquat. Toxicol.*, 2020, **229**, 105653.